Molecular Simulation of Separation of CO_2 from Flue Gases in Cu-BTC Metal-Organic Framework

Qingyuan Yang, Chunyu Xue, Chongli Zhong, and Jian-Feng Chen
Dept. of Chemical Engineering, Key Lab for Nanomaterials, Ministry of Education, Beijing University of Chemical Technology, Beijing 100029, China

DOI 10.1002/aic.11298
Published online September 28, 2007 in Wiley InterScience (www.interscience.wiley.com).

In this work, a computational study was performed on the adsorption separation of CO_2 from flue gases (mixtures of $CO_2/N_2/O_2$) in Cu-BTC metal-organic framework (MOF) to investigate the applicability of MOFs to this important industrial system. The computational results showed that Cu-BTC is a promising material for separation of CO_2 from flue gases, and the macroscopic separation behaviors of the MOF were elucidated at a molecular level to give insight into the underlying mechanisms. The present work not only provided useful information for understanding the separation characteristics of MOFs, but also showed their potential applications in chemical industry. © 2007 American Institute of Chemical Engineers *AIChE J,* 53: 2832–2840, 2007
Keywords: adsorption, separation, molecular modeling, flue gas, metal-organic framework

Introduction

As a primary contributor to the global climate change, commonly known as the "green house effect," the capture and sequestration of CO_2 from the exhausted gases by nanoporous adsorbents have been receiving significant attention in the recent years.[1] The excess CO_2 in atmosphere is largely due to the vast amount of the flue gases emitted from the combustion of carbon-based fossil fuels, and extensive studies have been conducted on the separation of CO_2 from flue gases in the conventional materials such as zeolites[2–5] and carbon materials.[6–8] Although some zeolite materials have been claimed to be most adequate for CO_2 separation from flue streams, it is difficult to regenerate them without significant heating which leads to low productivity and great expense.[9]

Owing to their flexibility to design through control of the architecture and chemical functionality of the pores, metal-organic frameworks (MOFs) have been recognized as a new family of nanoporous materials with various promising applications.[10–17] Among the various MOFs synthesized, Cu-BTC is a typical representative that shows promising applications to gas storage and mixture separation. Although several theoretical investigations have been carried out on the adsorption and diffusion of light gases or gas mixtures in this material, for example, the grand canonical Monte Carlo (GCMC) simulation study of the adsorption of Ar in Cu-BTC,[18] the adsorption[19] and diffusion[20,21] of light gases in Cu-BTC, the density functional theory (DFT) study of the interaction of C_2H_6 and C_2H_4 with several representative clusters of Cu-BTC,[22] and our previous studies of Cu-BTC performances for $CO_2/CH_4/C_2H_6$ and $CO_2/CH_4/H_2$ separations,[23,24] there was no such investigation on CO_2 separation from flue gas in this material, as well as in other MOFs. Thus, to compare with other nanoporous adsorbents as well as to explore the applicability of MOFs in this aspect, this work performed a computational study on the separation of CO_2 from flue gases using Cu-BTC. In this work, particular attention was paid to the competitive adsorption of the gas mixture ($CO_2/N_2/O_2$) consisting of three different quadrupolar molecules in Cu-BTC.

Correspondence concerning this article should be addressed to J.-F. Chen at chenjf@mail.buct.edu.cn.

Model and Computational Details

MOF structure

In this work, a well-known highly porous MOF, Cu-BTC first synthesized by Chui et al.[25] was adopted as a representative of MOFs. The structure model of Cu-BTC was constructed from the experimental XRD data[25] using Materials Visualizer,[26] and its unit cell is shown in Figure 1. As seen from Figure 1, Cu-BTC is a three-dimensional network with main channels of a square cross-section of ca. 9.0×10^{-10} m diameter and tetrahedral side pockets of ca. 5.0×10^{-10} m, which are connected to the main channels by triangular windows of ca. 3.5×10^{-10} m diameter. It should be pointed out that the crystal structure of Cu-BTC[25] includes axial oxygen atoms weakly bonded to the Cu atoms, which correspond to water ligands. Our simulations were performed on dry Cu-BTC with these oxygen atoms removed (activated Cu-BTC that is used in adsorption experiments), and thus the diameter of the triangular windows is ca. 4.6×10^{-10} m, which are wide enough to allow the studied adsorbate molecules to enter the pockets.

Force fields

Force fields play an important role in molecular simulations, and the adsorption behaviors of these quadrupolar adsorbates are extremely sensitive to the gradient of the electrostatic field inside the pores of Cu-BTC.[23] Thus, in the present work, the adsorbate CO_2 was modeled as a rigid linear triatomic molecule with three charged LJ interaction sites located at each atom. The LJ potential parameters for atom O ($\sigma_O = 3.05 \times 10^{-10}$ m and $\varepsilon_O/k_B = 79.0$ K) and atom C ($\sigma_C = 2.80 \times 10^{-10}$ m and $\varepsilon_C/k_B = 27.0$ K) in CO_2 molecule with C—O bond length $l = 1.16 \times 10^{-10}$ m were taken from the TraPPE force field developed by Potoff and Siepmann.[27] Partial point charges centered at each LJ site ($q_O = -0.35e$ and $q_C = 0.70e$) approximately represent the first-order electrostatic and second-order induction interactions. The represented CO_2 quadrupole moment ($Q = -1.51 \times 10^{-39}$ C m^2) by these partial point charges is slightly enhanced compared to the experimental value for an isolated CO_2 molecule ($Q = -1.47 \times 10^{-39}$ C m^2), but remains within the statistical uncertainty of the experimental measurement.[27] This potential model has been successfully used to model the adsorption of CO_2 in MOFs.[23,24]

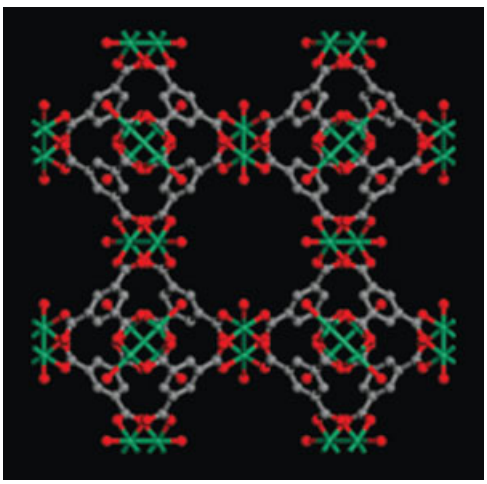

Figure 1. Unit cell crystal structure of Cu-BTC framework viewed along the [100] direction, showing nanochannels with fourfold symmetry (Cu, green; O, red; C, gray, and H atoms are omitted for clarity).

[Color figure can be viewed in the online issue, which is available at www.interscience.wiley.com.]

N_2 molecule was represented as a three-site model with two sites located at two N atoms and the third one located at its center of mass (COM). The site at each N atom was modeled by LJ interaction potential ($\sigma_N = 3.31 \times 10^{-10}$ m and $\varepsilon_N/k_B = 36.0$ K). The bond length between two N atoms is 1.10×10^{-10} m. In addition, to reproduce the measured gas-phase quadrupole moment of N_2 ($Q = -4.67 \times 10^{-40}$ C m^2), each N_2 molecule was assigned a negative charge on each N atom ($q_N = -0.482e$) and a positive charge at the COM site ($q_{COM} = 0.964e$).[27] These potential parameters were also taken from the TraPPE force field,[27] which have also been successfully adopted to simulate the adsorptions of pure N_2 and its mixture with CO_2 in zeolites.[2] The potential model employed for the adsorbate O_2 are similar to that for N_2. The bond length between two O atoms is 1.21×10^{-10} m. The LJ potential parameters of atom O ($\sigma_O = 3.02 \times 10^{-10}$ m and $\varepsilon_O/k_B = 49.0$ K) were suggested by Zhang and Siepmann,[28] and the partial charges ($q_O = -0.113e$, $q_{COM} = 0.226e$) were arranged to reproduce the experimental gas-phase quadrupole moment of O_2 ($Q = -1.33 \times 10^{-40}$ C m^2).[29] The above potential parameters have been successfully used to describe the vapor–liquid coexistence curve of pure O_2.[28] The interactions between various sites in the adsorbed molecules were calculated by the summation of LJ interactions and the electrostatic interactions, and all the LJ cross interaction parameters were determined by the Lorentz-Berthelot mixing rules.

For MOF material studied in this work, an atomistic representation was adopted. In this work, as before,[23,24] the all-atom OPLS[30] (OPLS-AA) force field was adopted to calculate the interactions between the adsorbate molecules and the atoms in the framework of the MOF material. Since the widely used Lorentz-Berthelot combining rules were adopted in the TraPPE force field to increase its transferability, the same combining rules were also used to calculate the LJ cross parameters describing the interactions of the CO_2 molecules with the framework atoms in the MOFs for consistency.

Simulation details

The conventional GCMC simulation was employed to calculate the adsorption of pure components and their mixtures in MOF materials. For pure components, the algorithm involves four types of trial moves: attempts to translate a molecule, attempts to rotate a molecule, attempts to create a new molecule, and attempts to delete an existing molecule. For mixtures, in order to speed up the equilibrium, an additional type of trial, attempts to exchange molecular identity, is also included. The structure of the unit cell of Cu-BTC was built from the XRD data using Materials Visualizer. The

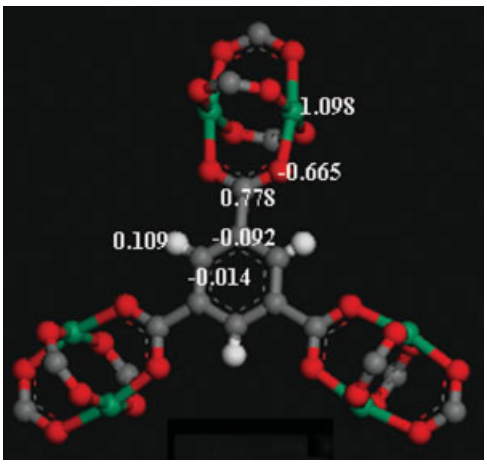

Figure 2. Model cluster of Cu-BTC used for the calculation of atomic partial charges (Cu, green; O, red; C, gray, and H, white).

[Color figure can be viewed in the online issue, which is available at www.interscience.wiley.com.]

number of the unit cells adopted in the simulation cell varied from $2 \times 2 \times 2$ to $3 \times 3 \times 3$ so that enough molecules were accommodated to guarantee the simulation accuracy. The framework was assumed to be rigid in all simulations. A cutoff radius of 1.5×10^{-9} m was applied to the LJ interactions, and the long-range electrostatic interactions were handled using the Ewald summation technique.[31] Periodic boundary conditions were applied in all three dimensions. For each state point, GCMC simulations consisted of 1×10^7 steps to guarantee equilibration followed by 1×10^7 steps to sample the desired thermodynamic properties were performed. As all the atoms in the adsorbent were assumed to be fixed in their crystallographic structure, the potential energies between an adsorbate and the adsorbent were initially tabulated on a series of three-dimensional grid points with grid spacing 1.5×10^{-11} m. During the simulations, the potential energy at any position in the adsorbent was determined by interpolation. To estimate the statistical uncertainty, the production phase of each state point was divided into 10 blocks and the standard deviation of the block average was calculated. The uncertainties on the final results, including the ensemble averages of the number of adsorbate molecules in the simulation cell and the total potential energy, were estimated on average to be within $\pm 2\%$.

In addition, the chemical potentials needed in the GCMC simulations were calculated from NPT ensemble Monte Carlo simulation using the test-particle insertion method.[32] Based on the simulated chemical potentials at various pressures, relationships between pressure and chemical potential were established to convert pressures to chemical potentials, and vice versa.

Results and Discussion

Atomic partial charge calculation

In all simulations, the atomic partial charges of Cu-BTC are required as input parameters. The model cluster of Cu-BTC used for atom partial charge calculation is shown in Figure 2. The terminations for this cluster were saturated with methyl groups. The electrostatic charges were used as the atomic partial charges, and the ChelpG method was adopted, which has been recognized as the most popular and reliable electrostatic charge calculation method.[33] DFT calculations using the UB3LYP functional were carried out to compute the atomic partial charges, and the basis set LANL2DZ was used for Cu atoms, while 6-31+G* for rest of the atoms. For heavy atoms, effective core potential (ECP) is often chosen in ab initio calculations to reduce the amount of necessary computation, and LANL2DZ is a collection of double-ξ basis sets, which is one of the most common ECP basis sets for complexes involving transition metal elements.[34] That is why we selected this basis set for Cu atoms. The calculations were performed using the GAUSSIAN 03 suite of programs,[35] and the calculated results are also shown in Figure 2.

Refinement of part OPLS-AA force field parameters

Since the parameters of the OPLS-AA force field were developed for liquid simulations, the existing parameters may not properly represent the interactions of the atoms of the solid MOF materials with the adsorbate molecules. Therefore, parts of the OPLS-AA force field parameters were refined.

In our previous work,[23] the potential parameters for the interactions between CO_2 molecules and the Cu-BTC framework have been obtained, as shown in Table 1. To better represent the adsorption isotherms of pure N_2 and O_2 in Cu-BTC at 295 K, the energy parameters of oxygen atoms

Table 1. Potential Parameters for the Atoms in the Framework of Cu-BTC

		ε/k, K		
Atom	σ, m	For Carbon Dioxide	For Nitrogen	For Oxygen
O	2.96×10^{-10}*	73.98†	63.41‡	52.84‡
$C_{arboxyl}$	3.75×10^{-10}*	44.91†	39.63‡	31.75‡
$C_{Benzene}$	3.55×10^{-10}*	35.23*	35.23*	24.66‡
$H_{Benzene}$	2.42×10^{-10}*	15.10*	15.10*	15.10*
Cu	3.11×10^{-10}§	2.52§	2.52§	2.52§

*Taken from the OPLS-AA force field of Jorgensen et al.[30]
†Taken from our previous work.[23]
‡Obtained in this work.
§Taken from the all-atom UFF force field (they are missed in the OPLS-AA force field).

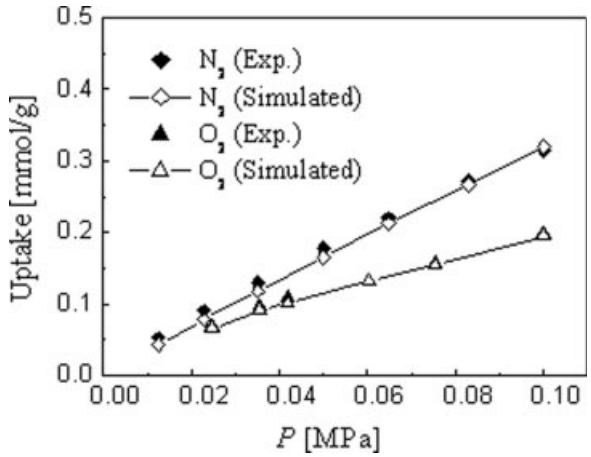

Figure 3. Comparison of simulated and experimental[36] adsorption isotherms of pure N_2 and O_2 in Cu-BTC at 295 K.

and carbon in carboxyl group in the Cu-BTC framework were adjusted for N_2, while those parameters of oxygen atoms and carbon in carboxyl as well as carbon atom in phenyl group were adjusted for O_2. All the potential parameters for N_2 and O_2 are shown in Table 1. Figure 3 demonstrates that the obtained parameters enable good reproductions of the corresponding experimental results[36] of pure N_2 and O_2 adsorptions in Cu-BTC, respectively.

To reveal the adsorption behaviors of gases in Cu-BTC at a molecular level, the snapshots of the structures of Cu-BTC with adsorbed gases were examined. Since the adsorption behavior is the same for CO_2, N_2, and O_2, only three snapshots of the structures of Cu-BTC with adsorbed N_2 are given as examples in Figure 4. Obviously, gas molecules first occupy the smaller tetrahedron-shaped side pockets (Figure 4a), followed by the saturation of the pockets (Figure 4b), and then they start occupying the positions near the unsaturated Cu atoms as well as the larger square-shaped channels with further increasing pressure. The similar behavior has also been observed in zeolites such as mordenite with similar topology.[37]

Binary mixtures

With these refined parameters, simulations on the adsorption of mixtures were further performed. In this work, a simulated dry flue gas mixture suggested by Xu et al.[38] was used as the adsorbate which contains 14.9% CO_2, 80.85% N_2, and 4.25% O_2 in molar composition. For each binary mixture studied in this work, the molar ratio of the two components is normalized according to their corresponding ratio in the flue gas mixture. In separation processes, a good indication of the ability for separation is the selectivity of a porous material for different components in mixtures. The selectivity for component A relative to component B is defined by $S = (x_A/x_B)(y_B/y_A)$, where x and y are the molar fractions of the adsorbed and bulk phase, respectively.

CO_2/N_2 Mixture. The most important binary system involved in flue gas purification process is the CO_2/N_2 system, and a huge amount of investigations have been performed on this system using carbon and zeolite materials, both experimentally and theoretically. Therefore, we also focused our discussion on this system in this work. Figure 5a shows the simulated selectivity for CO_2 from the binary mixture of CO_2/N_2 with gas composition CO_2:N_2 = 0.156:0.844 in Cu-BTC at 298 K, as a function of the bulk pressure up to 5.0 MPa. Obviously, a monotonous increase of CO_2 selectivity with increasing pressure has been observed in the pressure range studied. This is due to the fact that within the pressure range studied, packing effects are not evident, and the energetic effect that favors the adsorption of CO_2 leads to the monotonous increase in CO_2 selectivity. Figure 5b shows the dependency of the simulated individual isosteric heat of adsorption for the binary mixture CO_2/N_2 at 298 K, as a function of the bulk pressure (loading). Figure 5b indicates that, under the studied pressure range, the isosteric heat of adsorption of CO_2 is larger than that of N_2, which accounts for the above energetically favored factor for CO_2 adsorption in Cu-BTC.

It has been commonly recognized that ideal adsorbed solution theory (IAST)[39] can give good predictions of gas mixture adsorption in many zeolites.[2,40] Thus, in this work IAST calculations were also performed to check if this is also the case for this mixture in Cu-BTC. Figure 5a shows that IAST

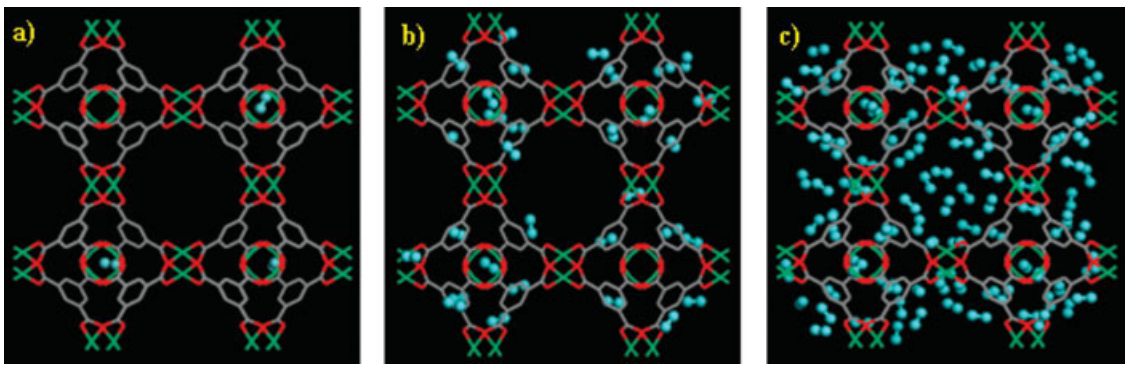

Figure 4. Snapshots of the structures of Cu-BTC with adsorbed N_2 molecules at three pressures: (a) P = 0.1 MPa, (b) P = 1.0 MPa, (c) P = 3.0 MPa (Cu-BTC framework is shown in line style with atoms H omitted for clarity; N_2: aqua ball-stick style).

[Color figure can be viewed in the online issue, which is available at www.interscience.wiley.com.]

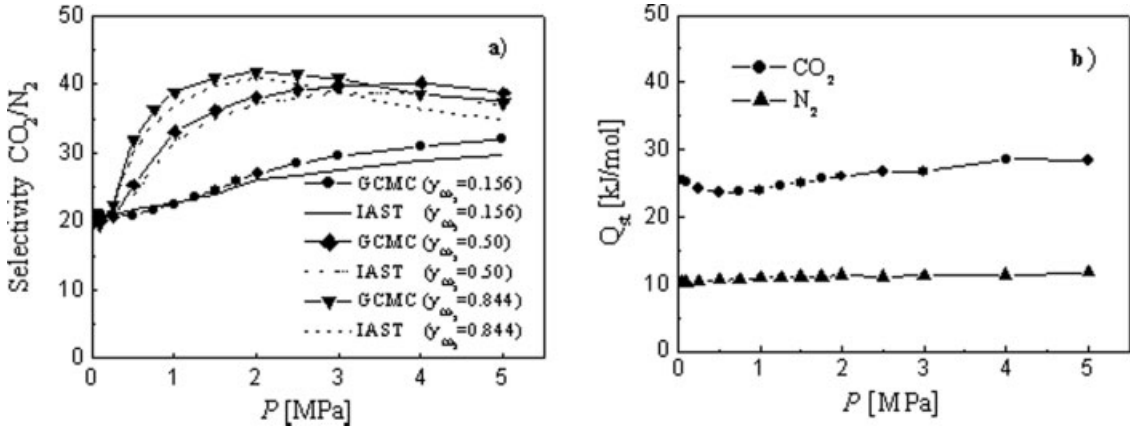

Figure 5. (a) Selectivity for CO_2 from binary mixtures of CO_2/N_2 with three gas compositions in Cu-BTC at 298 K; (b) the individual isosteric heat of adsorption for binary mixture CO_2/N_2 in Cu-BTC at 298 K, gas composition: 15.6% CO_2 and 84.4% N_2.

gives good agreement with the GCMC simulations for this binary mixture. To further test the applicability of IAST, GCMC simulations were performed for two additional gas compositions, and compared with those of the corresponding IAST calculations, as shown in Figure 5a. In all the cases, good agreement between GCMC simulation and IAST calculation was obtained, indicating that IAST is applicable to predict the adsorption behavior of CO_2/N_2 mixture in Cu-BTC. Therefore, the selectivity as a function of gas phase pressure and composition was mapped systematically using IAST for this system, as shown in Figure 6a. As expected, the selectivity is nearly independent of gas composition at low pressures, and its value is in good agreement with the ratio of the Henry's law constants K_H for the two adsorbed species ($K_H \cdot (CO_2)/K_H \cdot (N_2) = 20.1$). While the pressure increases, packing effects start to work, leading to a more complex gas composition dependency of selectivity. Finally, it should be noted that, to accurately apply IAST for this system in Cu-BTC, additional experimental adsorption data for pure adsorbates up to high pressures at the examined temperatures are required.

Since the competitive adsorptions of CO_2 and N_2 are extremely sensitive to the gradient of the electrostatic field inside the pores of Cu-BTC, GCMC simulations were further carried out to calculate the CO_2 selectivity from CO_2/N_2 mixture by switching off all the electrostatic interactions between the adsorbate molecules and the framework of Cu-BTC (without EI), as shown in Figure 6b. To make a comparison, the simulated results presented in Figure 5 (Full EI, with the electrostatic interactions) are also shown in Figure 6b. Evidently, the electrostatic field inside the pores of Cu-BTC indeed largely enhances the separation of gases with different quadrupole moments.

Separation of CO_2 from mixture CO_2/N_2 has also been widely investigated in other nanoporous materials. For example, at room temperature and moderate pressure, the selectivity is 15.3 in activated carbon Norit R1,[7] 30 in silicalite,[2] 100 in ITQ-3,[2] 14.0 in MFI-type zeolites,[3] 18.8 in zeolites

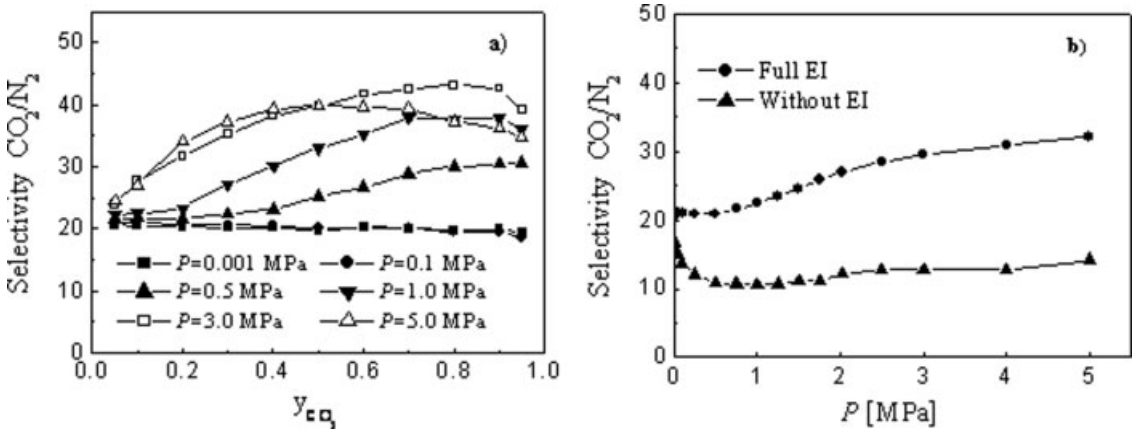

Figure 6. (a) IAST calculations for the CO_2 selectivity from binary mixture of CO_2/N_2 as a function of gas composition and pressure in Cu-BTC at 298 K; (b) effect of the electrostatic field inside the pores of Cu-BTC on the selectivity of CO_2 from the binary mixture of CO_2/N_2 at 298 K, gas composition: 15.6% CO_2 and 84.4% N_2.

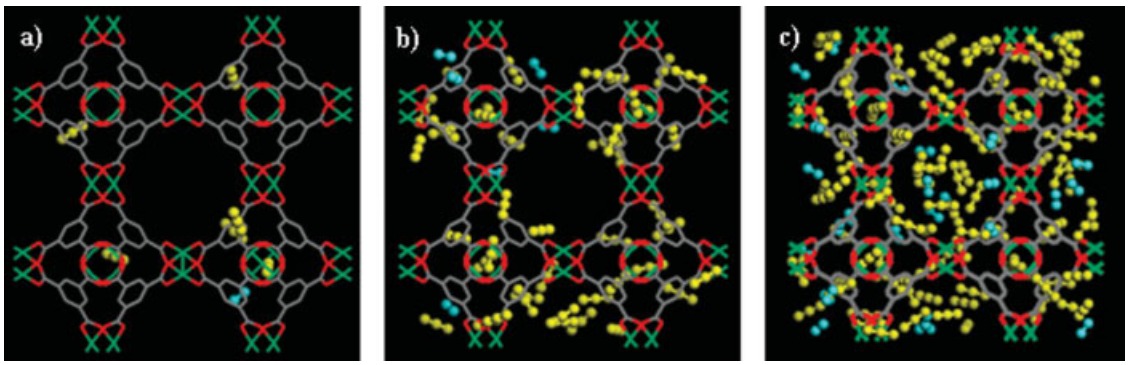

Figure 7. Snapshots of the structures of Cu-BTC with adsorbed binary mixture of CO_2/N_2 with gas composition CO_2:N_2 = 15.6:84.4 at three pressures: (a) P = 0.1 MPa, (b) P = 1.0 MPa, (c) P = 5.0 MPa (Cu-BTC framework is shown in line style with atoms H omitted for clarity; CO_2, yellow ball-stick style; N_2, green ball-stick style).

[Color figure can be viewed in the online issue, which is available at www.interscience.wiley.com.]

Na-4A,[4] and 20 in FAU-type zeolites.[5] Thus, a conclusion could be drawn from Figure 5a that Cu-BTC is a promising alternative material for this purpose.

The typical snapshots of Cu-BTC with adsorbed mixture CO_2/N_2 are shown in Figure 7. Clearly, up to 1.0 MPa both the molecules occupy mainly the side pockets, while with pressure further increased, they also occupy the positions near the unsaturated Cu atoms and the channels. Figure 7c shows up to 5.0 MPa, the channels are not packed tightly, and thus the packing effects are not evident within the pressure range studied. Furthermore, to investigate whether a competitive location exists for CO_2 and N_2 molecules near the unsaturated Cu atoms in the framework of Cu-BTC, the radical distribution functions $G(r)$ of the COM of the individual adsorbate molecules in this adsorbed mixture from the unsaturated Cu atoms were calculated. As seen from Figure 8, due to the stronger interaction strength with the unsaturated Cu atoms, the larger quadrupolar CO_2 molecules are

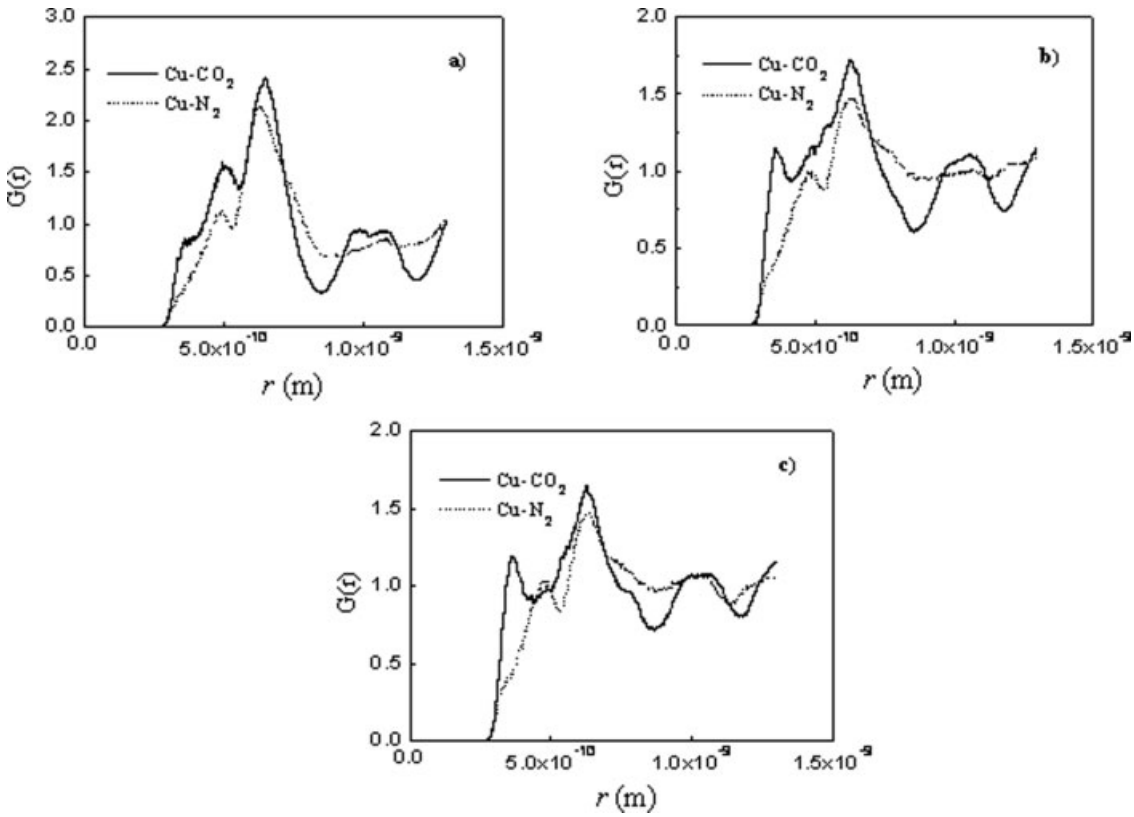

Figure 8. Radical distribution functions between the unsaturated Cu atoms and the center of mass of the individual adsorbate molecules in the adsorbed mixture CO_2/N_2 at three pressures: (a) P = 0.1 MPa, (b) P = 2.0 MPa, (c) P = 5.0 MPa.

Gas composition: 15.6% CO_2 and 84.4% N_2.

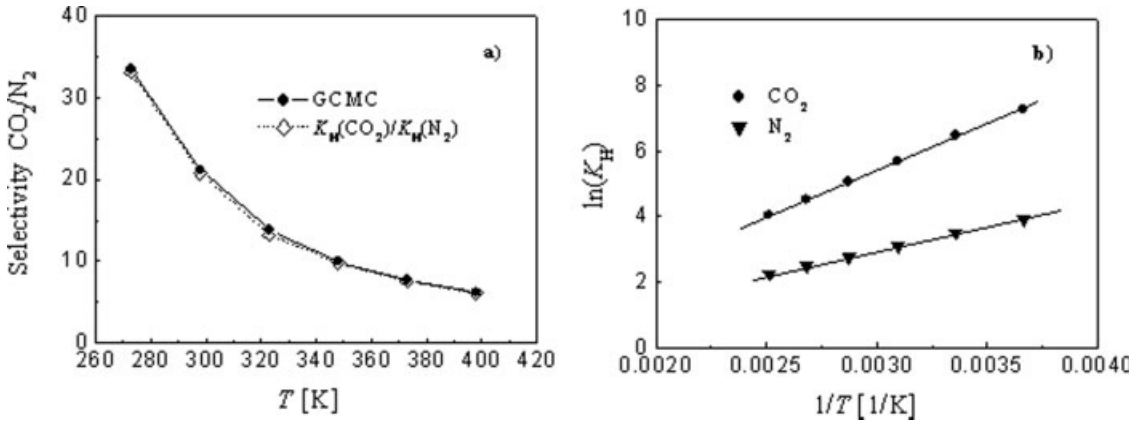

Figure 9. (a) Temperature dependency of CO_2 selectivity from mixture CO_2/N_2 in Cu-BTC at 0.1 MPa (gas composition: 15.6% CO_2 and 84.4% N_2); (b) temperature dependency of the Henry's law constant for pure CO_2 and N_2.

adsorbed much closer to the Cu atoms than N_2 molecules at all the examined pressures, which indicates that there is a preferential location of CO_2 molecules near the unsaturated Cu atoms.

For practical applications, it is interesting to investigate the dependency of the selectivity on the adsorption temperature. Figure 9a shows that the selectivity decreases approximately exponentially with increasing temperature. The simulated result suggests that the temperature, in addition to the bulk pressure, is also an important factor that should be considered in optimizing the process for adsorption separation of gas mixtures.

To give insight into the behavior of the temperature dependency of selectivity, Figure 9a also shows the ratio of K_H for the individual species at the corresponding temperatures. The good agreement between the calculations from the two methods indicates that the selectivity at low pressure region is defined by the ratio of K_H for the individual species. Moreover, Figure 9b gives the dependency of K_H in logarithmic coordinates for pure CO_2 and N_2 on the inverse temperature. The linear relationship illustrates that these Henry's law constants are related to temperature in an Arrhenius fashion through the isosteric heat of adsorption, consistent with the general behavior observed in other materials.

CO_2/O_2 Mixture. The selectivity of CO_2 from the binary mixture of CO_2/O_2 with gas composition CO_2:O_2 = 77.8:22.2 was further studied in Cu-BTC. The simulated results at room temperature are shown in Figure 10a, as a function of the bulk pressure up to 5.0 MPa. Obviously, it shows different behavior with that of CO_2/N_2 (Figure 5a) in the pressure range studied. This can be attributed to the difference in compositions. For CO_2/N_2 the composition is CO_2:N_2 = 15.6:84.4, whereas for CO_2/O_2 the composition is CO_2:O_2 = 77.8:22.2. The larger ratio of CO_2 in the binary mixture of CO_2/O_2 leads to more CO_2 molecules presented in the systems at the same pressure, resulting in a more significant packing effect. To illustrate this clearly, the snapshot of Cu-BTC with adsorbed CO_2/O_2 at 3.0 MPa is shown in

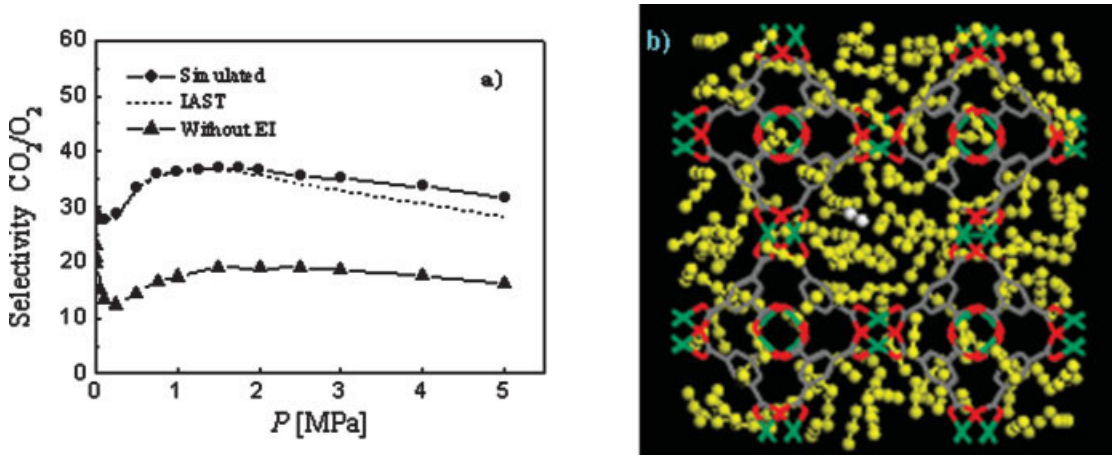

Figure 10. (a) Selectivity for CO_2 from the mixture CO_2/O_2 in Cu-BTC at 298 K; (b) snapshot of the structure of Cu-BTC with adsorbed binary mixture of CO_2/O_2 with gas composition CO_2:N_2 = 77.8:22.2 at P = 3.0 MPa (Cu-BTC framework is shown in line style with atoms H omitted for clarity; CO_2, yellow ball-stick style; O_2, white ball-stick style).

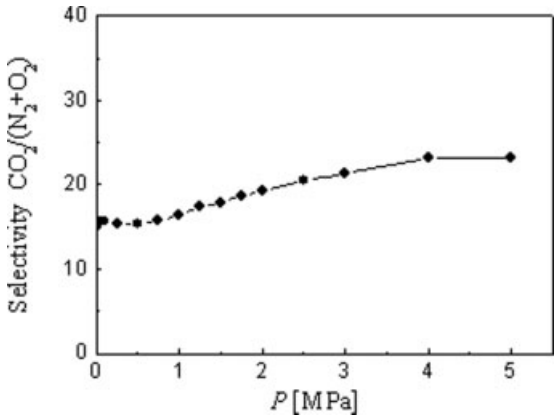

Figure 11. Selectivity of CO_2 from ternary mixture CO_2/N_2/O_2 in Cu-BTC at 298 K.

Gas composition: 14.9% CO_2, 80.85% N_2 and 4.25% O_2.

Figure 10b. Obviously, the channel is packed tightly, much tighter than the CO_2/N_2 system even at 5.0 MPa. This illustrates that gas composition is also a factor that should be considered in the design of separation conditions. Furthermore, it was found that the radical distribution functions $G(r)$ for the individual adsorbate molecules in the mixture CO_2/O_2 from the unsaturated Cu atoms were similar to those for the mixture CO_2/N_2 shown in Figure 8, demonstrating a preferential location for CO_2 molecules near the unsaturated Cu atoms relative to O_2 molecules.

Figure 10a also shows that the results obtained by IAST calculations give good agreement with those of the GCMC simulations. In addition, it is also found that the relationship between the selectivity and gas composition as well as pressure is similar to the results shown in Figure 6a, and thus this plot was omitted. Further, the impact of the electrostatic field inside the pores of Cu-BTC on the CO_2 selectivity from the mixture of CO_2/O_2 was also considered by switching off all the electrostatic interactions between CO_2 molecules as well as O_2 molecules and the framework of Cu-BTC (without EI). As seen from Figure 10a, the calculated selectivities are greatly reduced relative to the results with full electrostatic interactions. Thus, together with the previous results for the mixture of CO_2/N_2, this work shows that electrostatic field inside the pores of Cu-BTC is very important for the mixtures composed of quadrupolar molecules.

Ternary mixture

Simulations on the adsorption of the ternary mixture CO_2/N_2/O_2 that contains 14.9% CO_2, 80.85% N_2, and 4.25% O_2 was further performed in Cu-BTC at 298 K. The simulation results show that the selectivity between each two components is similar to that in the corresponding binary systems, and thus these plots were omitted. Since the purpose of purification of flue gas is to remove CO_2 from the mixture mainly composed of CO_2, N_2, and O_2, it is important to know the overall selectivity of CO_2 from the ternary mixture. Figure 11 demonstrates that the selectivity of CO_2 from the ternary mixture shows similar behavior as that of the binary mixture of CO_2/N_2. This is not unexpected since the ternary mixture contains only a few percent of O_2.

Finally, it should be pointed out that the molecular dynamics simulations of Skoulidas and Sholl demonstrate that diffusivities of light gases in MOFs are similar to those in zeolites,[21] indicating that the diffusion rate is not a significant factor to limit charging or discharging times in MOFs. Therefore, the separation of CO_2 from the mixture of CO_2/N_2/O_2 using Cu-BTC should be an equilibrium-based process with high selectivities that may find practical applications.

Conclusion

In this work, a computational study was performed on the adsorption separation of $CO_2/N_2/O_2$ mixtures in the well-known MOF, Cu-BTC. The results showed that MOFs are promising materials for separating CO_2 from flue gases. In addition to the bulk pressure, temperature and gas composition are also important factors in optimizing the process for adsorption separation of gas mixtures. Furthermore, this work shows that the electrostatic field inside the pores of Cu-BTC is very important for the selective behaviors of the mixtures composed of quadrupolar molecules. The simulation results not only revealed some separation characteristics of MOFs, but also illustrated that MOFs may find wide applications in gas mixture separations in chemical industry.

Acknowledgments

The financial supports of the NSFC (Nos. 20676004, 20325621, 50642042) and the Natural Science Foundation of Young Teacher of BUCT (QN0604) are greatly appreciated.

Literature Cited

1. Aaron D, Tsouris C. Separation of CO_2 from flue gas: a review. *Sep Sci Technol*. 2005;40:321–348.
2. Goj A, Sholl DS, Akten ED, Kohen D. Atomistic simulations of CO_2 and N_2 adsorption in silica zeolites: the impact of pore size and shape. *J Phys Chem B*. 2002;106:8367–8375.
3. Bernal MP, Coronas J, Menéndez M, Santamaría J. Separation of CO_2/N_2 mixtures using MFI-type zeolite membranes. *AIChE J*. 2004; 50:127–135.
4. Akten ED, Siriwardane RV, Sholl DS. Monte Carlo simulation of single and binary component adsorption of CO_2 and N_2 on zeolite 4A. *Energy Fuels*. 2003;17:977–983.
5. Seike T, Matsuda M, Miyake M. Preparation of FAU type zeolite membranes by electrophoretic deposition and their separation properties. *J Mater Chem*. 2002;12:366–368.
6. Jiang J, Sandler SI. Separation of CO_2 and N_2 by adsorption in C_{168} schwarzite: a combination of quantum mechanics and molecular simulation study. *J Am Chem Soc*. 2005;127:11989–11997.
7. Dreisbach F, Staudt R, Keller JU. High pressure adsorption data of methane, nitrogen, carbon dioxide and their binary and ternary mixtures on activated carbon. *Adsorption*. 1999;5:215–227.
8. Andrews R, Jagtoyen M, Grulke E, Lee KH, Mao ZA, Sinnott SB. In: Proceedings of the Sixth Applied Diamond Conference/Second Frontier Carbon Technology Joint Conference, Auburn, Alabama, 2001.
9. Bourrelly S, Llewellyn PL, Serre C, Millange F, Loiseau T, Férey G. Different adsorption behaviors of methane and carbon dioxide in the isotypic nanoporous metal terephthalates MIL-53 and MIL-47. *J Am Chem Soc*. 2005;127:13519–13521.
10. Snurr RQ, Hupp JT, Nguyen ST. Prospects for nanoporous metal-organic materials in advanced separations processes. *AIChE J*. 2004; 50:1090–1095.
11. Rowsell JLC, Yaghi OM. Strategies for hydrogen storage in metal-organic frameworks. *Angew Chem Int Ed Engl*. 2005;44:4670–4679.

12. Kubota Y, Takata M, Matsuda R, Kitaura R, Kitagawa S, Kato K, Sakata M, Kobayashi TC. Direct observation of hydrogen molecules adsorbed in a microporous coordination polymer. *Angew Chem Int Ed Engl*. 2005;44:920–923.
13. Düren T, Sarkisov L, Yaghi OM, Snurr RQ. Design of new materials for methane storage. *Langmuir*. 2004;20:2683–2689.
14. Pan L, Olson DH, Ciemnolonski LR, Heddy R, Li J. Separation of hydrocarbons with a microporous metal–organic framework. *Angew Chem Int Ed Engl*. 2006;45:616–619.
15. Chen B, Liang C, Yang J, Contreras DS, Clancy YL, Lobkovsky EB, Yaghi OM, Dai S. A microporous metal-organic framework for gas-chromatographic separation of alkanes. *Angew Chem Int Ed Engl*. 2006;45:1390–1393.
16. Babarao R, Hu Z, Jiang JW, Chempath S, Sandler SI. Storage and separation of CO_2 and CH_4 in silicalite, C_{168} schwarzite, and IRMOF-1: a comparative study from Monte Carlo simulation. *Langmuir*. 2007;23:659–666.
17. Jiang J, Sandler SI. Monte Carlo simulation for the adsorption and separation of linear and branched alkanes in IRMOF-1. *Langmuir*. 2006;22:5702–5707.
18. Vishnyakov A, Ravikovitch PI, Neimark AV, Bülow M, Wang QM. Nanopore structure and sorption properties of Cu-BTC metal-organic framework. *Nano Lett*. 2003;3:713–718.
19. Garberoglio G, Skoulidas AI, Johnson JK. Adsorption of gases in metal organic materials: comparison of simulations and experiments. *J Phys Chem B*. 2005;109:13094–13103.
20. Skoulidas AI. Molecular dynamics simulations of gas diffusion in metal-organic frameworks: argon in CuBTC. *J Am Chem Soc*. 2004; 126:1356–1357.
21. Skoulidas AI, Sholl DS. Self-diffusion and transport diffusion of light gases in metal-organic framework materials assessed using molecular dynamics simulations. *J Phys Chem B*. 2005;109:15760–15768.
22. Nicholson TM, Bhatia SK. Electrostatically mediated specific adsorption of small molecules in metallo-organic frameworks. *J Phys Chem B*. 2006;110:24834–24836.
23. Yang QY, Zhong CL. Electrostatic-field-induced enhancement of gas mixture separation in metal-organic frameworks: a computational study. *ChemPhysChem*. 2006;7:1417–1421.
24. Yang QY, Zhong CL. Molecular simulation of carbon dioxide/methane/hydrogen mixture adsorption in metal-organic frameworks. *J Phys Chem B*. 2006;110:17776–17783.
25. Chui SS-Y, Lo SM-F, Charmant JPH, Orpen AG, Williams ID. A chemically functionallizable nanoporous material $[Cu_3(TMA)_2\ (H_2O)_3]_n$. *Science*. 1999;283:1148–1150.
26. Accelrys Inc. *Materials Studio*, 3.0 V. Accelrys Inc: San Diego, CA, 2003.
27. Potoff JJ, Siepmann JI. Vapor-liquid equilibria of mixtures containing alkanes, carbon dioxide, and nitrogen. *AIChE J*. 2001;47:1676–1682.
28. Zhang L, Siepmann JI. Direct calculation of Henry's law constants from Gibbs ensemble Monte Carlo simulations: nitrogen, oxygen, carbon dioxide, and methane in ethanol. *Theor Chem Acc*. 2006; 115:391–397.
29. Buckingham AD, Dunmurl DA. The quadrupole moments of some simple molecules. *J Am Chem Soc*. 1968;90:3104–3107.
30. Jorgensen WL, Maxwell DS, Tirado-Rives J. Development and testing of the OPLS all-atom force field on conformational energetics and properties of organic liquids. *J Am Chem Soc*. 1996;118:11225–11236.
31. Frenkel D, Smit B. *Understanding Molecular Simulation: From Algorithms to Applications*. San Diego: Academic Press, 2002.
32. Shing KS, Chung ST. Computer simulation methods for the calculation of solubility in supercritical extraction systems. *J Phys Chem*. 1987;91:1674–1681.
33. Heinz H, Suter UW. Structure and phase transitions of alkyl chains on Mica. *J Phys Chem B*. 2004;108:18341–18352.
34. Foguet-Albiol D, O'Brien TA, Wernsdorfer W, Moulton B, Zaworotko M J, Abbound KA, Christou G. DFT computational rationalization of an unusual spin ground state in an Mn_{12} single-molecule magnet with a low-symmetry loop structure (pNA). *Angew Chem Int Ed Engl*. 2005;44:897–901.
35. Frisch MJ, Trucks GW, Schlegel HB, Scuseria GE, Robb MA, Cheeseman, JR, Montgomery JA Jr, Vreven T, Kudin KN, Burant JC, Millam JM, Iyengar SS, Tomasi J, Barone V, Mennucci B, Cossi M, Scalmani G, Rega N, Petersson GA, Nakatsuji H, Hada M, Ehara M, Toyota K, Fukuda R, Hasegawa J, Ishida M, Nakajima T, Honda Y, Kitao O, Akai H, Klene M, Li X, Knox JE, Hratchian HP, Cross JB, Adamo C, Jaramillo J, Gomperts R, Stratmann RE, Yazyev O, Austin AJ, Cammi R, Pomelli C, Ochterski JW, Ayala PY, Morokuma K, Voth GA, Salvador P, Dannenberg JJ, Zakrzewski VG, Dapprich S, Daniels AD, Strain MC, Farkas O, Malick DK, Rabuck AD, Raghavachari K, Foresman JB, Ortiz JV, Cui Q, Baboul AG, Clifford S, Cioslowski J, Stefanov BB, Liu G, Liashenko A, Piskorz P, Komaromi I, Martin RL, Fox DJ, Keith T, Al-Laham MA, Peng CY, Nanayakkara A, Challacombe M, Gill PMW, Johnson B, Chen W, Wong MW, Gonzalez C, Pople JA. Gaussian 03. Gaussian, Inc.: Pittsburgh, PA, 2003.
36. Wang Q, Shen D, Bülow M, Lau M, Deng S, Fitch FR, Lemcoff NO, Semanscin J. Metallo-organic molecular sieve for gas separation and purification. *Microporous Mesoporous Mater*. 2002;55:217–230.
37. Nivarthi SS, Van Tassel PR, Davis HT, McCormick AV. Adsorption and energetics of xenon in mordenite: a Monte Carlo simulation study. *J Chem Phys*. 1995;103:3029–3037.
38. Xu XC, Song CS, Miller BG, Scaroni AW. Influence of moisture on CO_2 separation from gas mixture by a nanoporous adsorbent based on polyethylenimine-modified molecular sieve MCM-41. *Ind Eng Chem Res*. 2005;44:8113–8119.
39. Myers AL, Prausnitz JM. Thermodynamics of mixed gas adsorption. *AIChE J*. 1965;11:121–127.
40. Chen HB, Sholl DS. Efficient simulation of binary adsorption isotherms using transition matrix Monte Carlo. *Langmuir*. 2006;22: 709–716.

Manuscript received Mar. 7, 2007, revision received Jun. 1, 2007, and final revision received Aug. 3, 2007.